**SANDIA REPORT**
SAND2022-2572
Printed March 2022

Sandia National Laboratories

# Ellipsoidal Fitting Methodology for Defect Clusters in Gallium Arsenide

Brian D. Hehr

Prepared by
Sandia National Laboratories
Albuquerque, New Mexico
87185 and Livermore,
California 94550

Issued by Sandia National Laboratories, operated for the United States Department of Energy by National Technology & Engineering Solutions of Sandia, LLC.



Available to DOE and DOE contractors from
U.S. Department of Energy
Office of Scientific and Technical Information
P.O. Box 62
Oak Ridge, TN 37831

Telephone: (865) 576-8401
Facsimile: (865) 576-5728
E-Mail: reports@osti.gov
Online ordering: http://www.osti.gov/scitech

Available to the public from
U.S. Department of Commerce
National Technical Information Service
5301 Shawnee Rd
Alexandria, VA 22312

Telephone: (800) 553-6847
Facsimile: (703) 605-6900
E-Mail: orders@ntis.gov
Online order: https://classic.ntis.gov/help/order-methods/

## ABSTRACT

In assessing the initial spatial distribution of defects from neutron or heavy ion irradiation, it is useful to have a reliable, automated, and fast-running tool to evaluate characteristic metrics such as the number of sub-clusters or the overall cluster volume. The latter metric, for instance, can be utilized to estimate a reference neutron fluence level at which inter-cluster interaction effects begin to become significant. This paper details a methodology to fit an arbitrarily complex defect map with a set of ellipsoids (one per identified sub-cluster) in which the constituent defects of a sub-cluster are determined using fuzzy degree-of-membership analysis. Specifically, a parameterized model is developed for point defects in gallium arsenide. Cluster volume calculations based on the model are compared against convex hull and single-ellipsoid representations. Results show that the parameterized sub-cluster model begins to deviate from the two reference models at a recoil energy of about 100 keV in GaAs, with the convex hull and single-ellipsoid representations increasingly overestimating the volume thereafter.

## ACKNOWLEDGEMENTS

This work was funded under the Survivability element of the Advanced Simulation and Computing (ASC) Physics and Engineering Models (P&EM) program.

## CONTENTS

1. Introduction ..... 9
2. Methodology ..... 11
   2.1. Cluster Center Identification ..... 11
   2.2. Degree-of-Membership Assignment ..... 12
   2.3. Ellipsoidal Fitting ..... 13
3. Model Application to Gallium Arsenide ..... 15
4. Defect Map Volume Estimates in Gallium Arsenide ..... 25
5. Conclusions ..... 29

## LIST OF FIGURES

Figure 3-1. Point defect map #1 from a 10-keV PKA in GaAs ..... 16
Figure 3-2. RDF of defect map #1 ..... 16
Figure 3-3. Point defect map #2 from a 10-keV PKA in GaAs ..... 17
Figure 3-4. RDF of defect map #2 ..... 17
Figure 3-5. Mean number of cluster centers versus recoil energy in GaAs, as identified using RDF analysis ..... 19
Figure 3-6. Mean number of cluster centers versus recoil energy in GaAs, as evaluated using the subtractive clustering algorithm. Curves are labeled by value of *ra* (see Eq. (2.1)). ..... 19
Figure 3-7. Candidate defect map from 50 keV recoil ..... 21
Figure 3-8. Ellipsoidal sub-cluster fit to candidate defect map from 50 keV recoil ..... 21
Figure 3-9. Candidate defect map from 500 keV recoil ..... 22
Figure 3-10. Ellipsoidal sub-cluster fit to candidate defect map from 500 keV recoil: Upper portion ..... 22
Figure 3-11. Ellipsoidal sub-cluster fit to candidate defect map from 500 keV recoil: Lower portion ..... 23

Figure 4-1. Defect map from a 20 keV recoil in GaAs (top panel), fitted with sub-cluster 2-sigma ellipsoids (middle panel), and overlaid with the convex hull (bottom panel). Distances are in angstroms. ..... 26
Figure 4-2. Calculated mean volume of defect maps versus recoil energy in GaAs as a function of volume estimation methodology ..... 27
Figure 4-3. Histogram of ratio of convex hull versus single 2-sigma ellipsoid estimate of cluster volume in the recoil energy range of 1000 eV to 500 keV. ..... 28

## LIST OF TABLES

Table 2-1. Fraction of defects in ellipsoidal volume ..... 13

Table 3-1. Recoil energy sampling scheme. Recoil events were initiated in random directions. ..... 18

This page left blank

# ACRONYMS AND DEFINITIONS

| Abbreviation | Definition |
|---|---|
| PCA | Principal Component Analysis |
| PKA | Primary Knock-on Atom |
| MD | Molecular Dynamics |
| RDF | Radial Distribution Function |
| TRIM | Transport of Ions in Matter |

This page left blank

# 1. INTRODUCTION

Materials exposed to neutron radiation experience recoil-induced displacement damage in the form of point defects and possibly higher-order defective regions such as amorphous zones, voids, or dislocation loops. Once the energetic collision cascade phase has ended, these defects will exist in a quasi-stable state pending the commencement of longer-time-scale annealing processes. In general, the quasi-stable defects will exhibit intricate morphologies that are subject to a large degree of stochastic variability; however, in an averaged sense, clear trends in characteristic spatial metrics may be identified in a wide variety of materials as a function of the primary knock-on atom (PKA) recoil energy. At recoil energies up to ~ 10 keV, the residual point defects constitute a single cluster. Once this threshold recoil energy for sub-cluster formation is exceeded, a splitting of the defect positions into two distinct sub-clusters may be observed. At still higher energies, multiple sub-clusters form and the overall defect map tends to become highly skewed along the axis defined by the initial PKA recoil direction, with the sub-clusters often being separated by linear chains of point defects.

In certain applications—such as characterization of distinct sub-clusters within a point defect map, assessment of skewness in such a map, or evaluation of the volume occupied by a map (e.g. for gauging the onset of inter-cluster overlap / interaction effects as a function of neutron fluence)—it is beneficial to have the capability of deploying an automated, robust methodology for fitting well-defined geometric shapes to the defect map or to sub-entities comprising the map. The purpose of this paper is to detail a general fitting methodology for point defect maps, with energetic recoil-induced cascades in gallium arsenide utilized as an exemplar. Ellipsoids were chosen as the basis for geometric fitting due the assured mathematical correspondence between the scaling of the ellipsoidal semi-axes and the percentage of point defect coverage under principal component analysis (PCA).

This page left blank

# 2. METHODOLOGY

The process of fitting ellipsoids to a defect map was comprised of the following steps:

1. Identification of the number of cluster centers via a subtractive clustering algorithm
2. Optimization of the cluster center positions, and assignment of a degree-of-membership of each defect to each cluster center, via fuzzy c-means clustering analysis
3. Fitting of an ellipsoid to each of the identified clusters, with only those defects exceeding a predetermined threshold degree-of-membership included in the fit

which are described in more detail in the respective sub-sections below.

## 2.1. Cluster Center Identification

To identify the number of cluster centers, a subtractive clustering algorithm was employed. Subtractive clustering—a modification of the mountain clustering method [1]—refers to an iterative process in which each data point is considered as a candidate cluster center. First, the density measure at each point is evaluated as:

$$D_i = \sum_{j=1}^{N_d} \exp\left( -\frac{4\left\| \mathbf{r}_i - \mathbf{r}_j \right\|^2}{r_a^2} \right) \tag{2.1}$$

where $\mathbf{r}_i$ is the position vector of defect $i$, $N_d$ is the total number of defects, and $r_a$ is a constant defining the neighborhood in which other defects contribute significantly to the density measure at defect $i$. The point with the highest density measure is designated as a cluster center. Following this designation, the density measure associated with every other point is adjusting via the following equation:

$$D_i^{'} = D_i - D_c \exp\left( -\frac{4\left\| \mathbf{r}_i - \mathbf{r}_c \right\|^2}{r_b^2} \right) \tag{2.2}$$

where $D_c$ and $\mathbf{r}_c$ are the density measure and position, respectively, of the designated cluster center, and $r_b$ defines the neighborhood about the newly-identified cluster center in which substantial reductions in the density measure will take place. The point with the next-highest density measure becomes the next cluster center, and the selection process continues until a suitable number of centers have been identified.

For the purposes of the present study, $r_b$ was set to $1.25r_a$, and $r_a$ itself was determined through the fitting process described in section 3.

## 2.2. Degree-of-Membership Assignment

In general, a defect either can be uniquely associated with a specific cluster or can be affiliated with multiple cluster centers in a fuzzy (non-binary) manner. The degree of membership is quantifiable via the membership matrix, **U**, an $N_d$ x $N_c$ matrix in which each element consists of a number between 0 and 1 specifying the degree of membership of defect *i* to cluster center *k* [2]. The membership matrix is subject to the constraint:

$$\sum_{k=1}^{N_c} U_{ik} = 1 \tag{2.3}$$

which is effectively a normalization condition of the membership partition. A cost function is then associated with a collection of defects as:

$$C = \sum_{k=1}^{N_c} \sum_{i=1}^{N_d} U_{ik}^m \left\| \vec{r}_i - \vec{r}_k \right\|^2 \tag{2.4}$$

A minimum is reached in the cost function when:

$$\vec{r}_k = \frac{\sum_{i}^{N_d} U_{ik}^m \cdot \vec{r}_i}{\sum_{i}^{N_d} U_{ik}^m} \tag{2.5}$$

and:

$$U_{ik} = \frac{1}{\sum_{l=1}^{N_c} \left( \frac{\left\| \vec{r}_i - \vec{r}_l \right\|}{\left\| \vec{r}_l - \vec{r}_k \right\|} \right)^{2/(m-1)}} \tag{2.6}$$

The procedure to converge on a membership matrix and a set of cluster center positions is to:

1. Initialize the membership matrix with random numbers between 0 and 1, subject to the constraint in Eq. (2.3).
2. Compute the cluster center positions using Eq. (2.5).
3. Compute a new membership matrix using Eq. (2.6).
4. Calculate the cost function from Eq. (2.4), exiting the iterative process if the cost value is either below a given threshold or if its change from the previous iteration is below a given tolerance.
5. Repeat steps 2 – 4

In this study, the weighting exponent, *m*, was set to 2.

## 2.3. Ellipsoidal Fitting

For the purpose of fitting a geometric shape to a collection of point defects (the "collection" being defined herein as the defects affiliated with an identified cluster center), ellipsoids are an attractive option due to a combination of generality and simplicity of mathematical representation. Details of the principal component analysis (PCA) approach are discussed in [3]. Briefly, the unit vectors defining the ellipsoidal semi-axes and the squares of the axis lengths are equal to the eigenvectors and eigenvalues, respectively, of the defect position covariance matrix. In particular, the computed semi-axis lengths correspond to the standard deviations (σ) of the defect positions as projected onto the respective axes. The aforementioned procedure, by default, will result in a 1σ scaling of the semi-axes under the assumption of a normal distribution of defects about each semi-axis. If the semi-axes are scaled by a factor *N* beyond the 1σ values, then the fraction of defects contained within the ellipsoidal volume is given by:

$$frac = 8\int_0^{\pi/2} d\phi \int_0^{\pi/2} d\theta \int_0^{N} d\rho \left( \frac{\rho^2}{(2\pi)^{3/2}} \sin\theta \right. \tag{2.7}$$

$$\left. \cdot \exp\left[ \frac{-(a\rho\cos\phi\sin\theta)^2}{2a^2} \right] \exp\left[ \frac{-(b\rho\sin\phi\sin\theta)^2}{2b^2} \right] \exp\left[ \frac{-(c\rho\cos\theta)^2}{2c^2} \right] \right)$$

$$frac = 4\pi \int_0^{N} d\rho \frac{\rho^2}{(2\pi)^{3/2}} \cdot \exp\left[ \frac{-\rho^2}{2} \right] \tag{2.8}$$

where *a*, *b*, and *c* are the semi-axis lengths and *rho*, *theta*, and *phi* are generalized spherical coordinates. Eq. (2.7) is essentially a volume integration over the ellipsoid as weighted by the probability density of finding a defect within each volume element. Integrations of up to 3σ are tabulated in Table 2-1.

**Table 2-1. Fraction of defects in ellipsoidal volume vs. sigma scaling of semi-axes**

| Scaling | Defect Coverage Fraction |
|---|---|
| 1σ | 0.199 |
| 2σ | 0.739 |
| 3σ | 0.971 |

This page left blank

# 3. MODEL APPLICATION TO GALLIUM ARSENIDE

In the practical application of the cluster assignment and geometric fitting methodology described in Section 2, two immediate issues arise: 1) how to utilize the degree-of-membership information within the ellipsoidal fitting process, and 2) how to determine the constant, $r_a$, in Eq. (2.1).

Regarding issue 1), the fitting process detailed in Section 2.3 operates under the assumption that all point defects are weighted equally. Rather than incorporate all defect positions in the fitting of a given sub-cluster by attempting to modulate their relative contributions by degree-of-membership, it was decided that those defects falling below a specified cutoff value would be eliminated from consideration. Specifically, defects with a degree-of-membership above $exp(-2)$ were incorporated into a $2\sigma$ ellipsoidal fit of the sub-cluster, while those falling short of the $exp(-2)$ threshold were ignored. The $exp(-2)$ cutoff was chosen based on the $2\sigma$ value of a notional exponential attenuation function in degree-of-membership versus distance from a cluster center.

To address issue 2), it was decided that the constant $r_a$ would be chosen to ensure consistency with the threshold recoil energy for sub-cluster formation in GaAs. An implication of this approach is that an independent means must be available for establishing a reference value of the sub-cluster formation energy. In the present study, the sub-cluster formation energy was designated as the recoil energy at which the radial distribution function (RDF) of the defect positions was observed to split into two distinct peaks, with "distinct" defined as possessing a minimum peak prominence of 5. The peak prominence is affected by the spatial separation of the sub-cluster centers, as well as by the characteristic dimensions of the sub-clusters themselves.

The RDF is defined by:

$$g(r) = \frac{1}{\eta N_d} \sum_{i=1}^{N_d} \sum_{j \neq i}^{N_d} \left\langle \delta\left(r + r_j - r_i\right) \right\rangle \tag{3.1}$$

where $\eta$ is a mean (background) defect density. The normalization factors preceding the double summation in Eq. (3.1) are irrelevant in this case because the peak splitting phenomenon of interest is discernible via the basic functional profile.

Figure 3-1 and Figure 3-3 show the defects maps from two independent recoil events at a PKA energy of 10 keV. Only a single cluster can be visually discerned in the former figure, whereas two distinct clusters, with an adjoining linear chain of defects, are apparent in the latter. RDFs corresponding to Figure 3-1 and Figure 3-3 are illustrated in Figure 3-2 and Figure 3-4 respectively; the single-peaked versus double-peaked behavior of the RDFs is seen to accord well with the visually obvious distinction between the single cluster and the two sub-clusters.

To evaluate the threshold energy of sub-cluster formation, defect map simulations were carried out at the recoil energies and sample sizes given in Table 3-1. The MARLOWE binary collision code ([4]-[7]) was used to simulate the collision cascade process and to obtain the quasi-stable defect maps given a PKA recoil energy and a randomly chosen recoil direction. Details of the MARLOWE calculations may be found in [8].

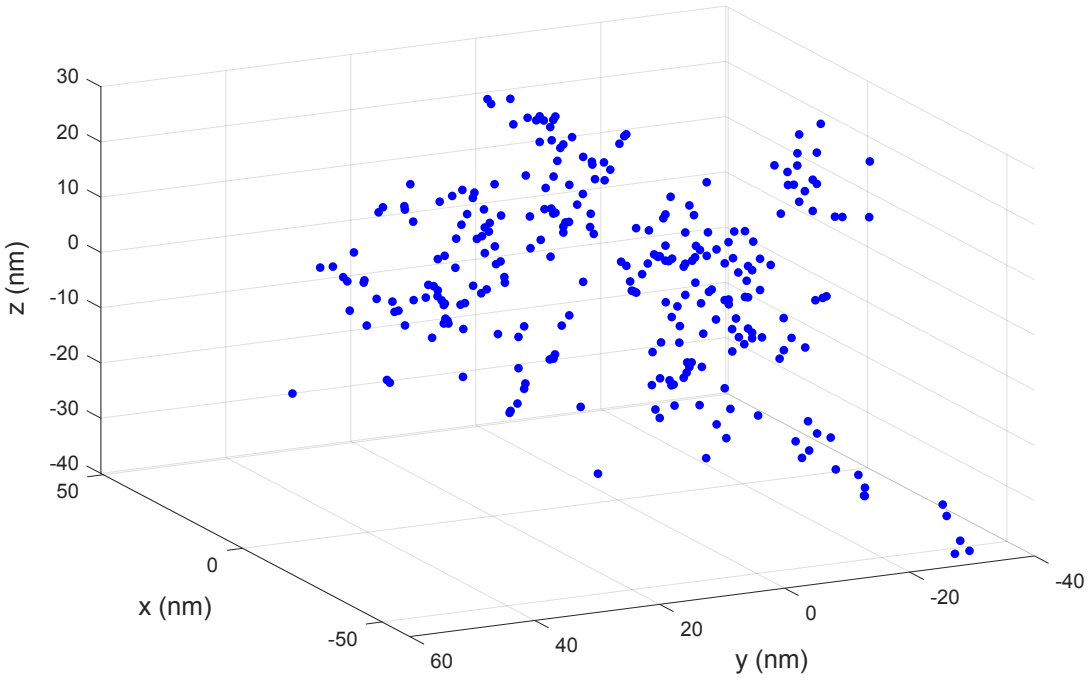


**Figure 3-1. Point defect map #1 from a 10-keV PKA in GaAs**

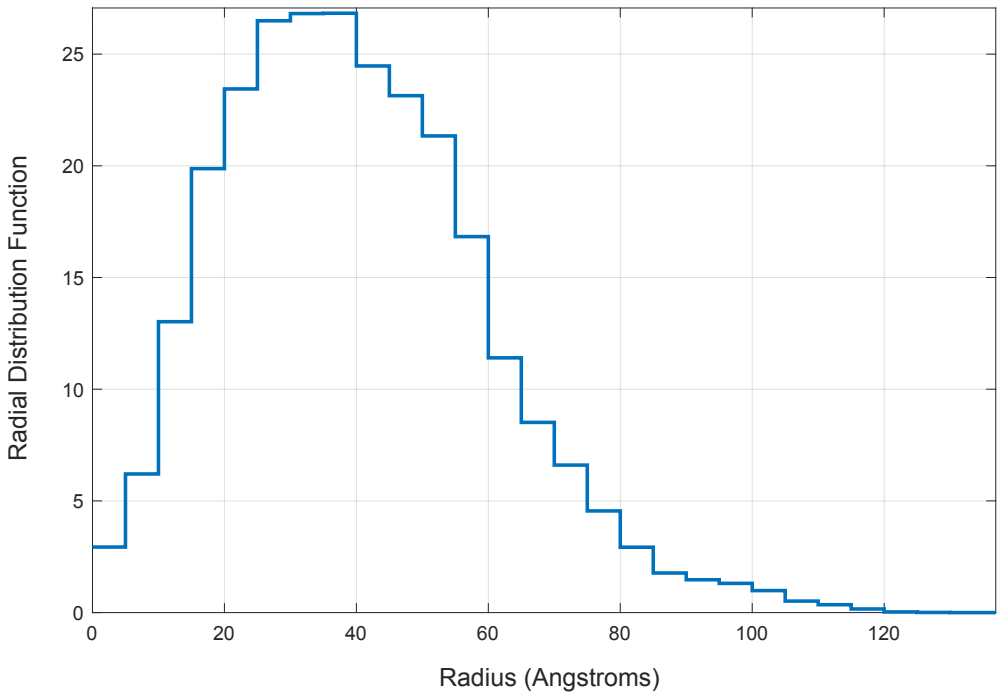


**Figure 3-2. RDF of defect map #1**

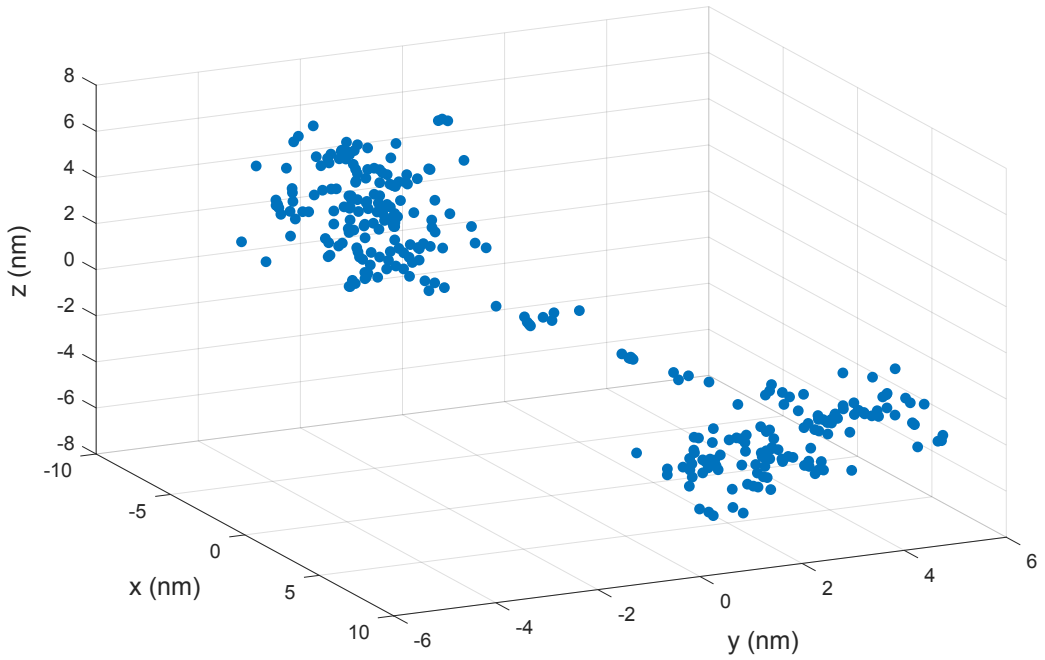


**Figure 3-3. Point defect map #2 from a 10-keV PKA in GaAs**

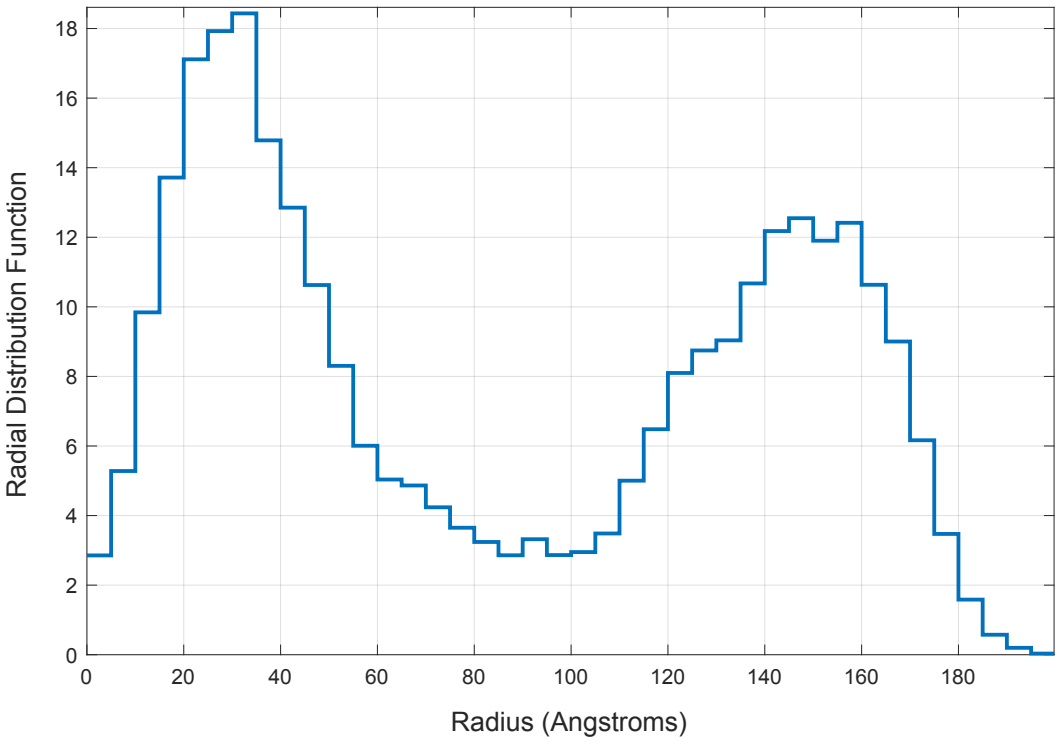


**Figure 3-4. RDF of defect map #2**

**Table 3-1. Recoil energy sampling scheme. Recoil events were initiated in random directions.**

| Recoil Energy (eV) | Realizations (#) | Recoil Energy (eV) | Realizations (#) | Recoil Energy (eV) | Realizations (#) |
|---|---|---|---|---|---|
| 100 | 500 | 3000 | 500 | 50000 | 500 |
| 200 | 500 | 5000 | 500 | 100000 | 500 |
| 300 | 500 | 10000 | 500 | 200000 | 500 |
| 1000 | 500 | 20000 | 500 | 300000 | 500 |
| 2000 | 500 | 30000 | 500 | 500000 | 500 |

Employing the RDF-based cluster quantification methodology, the mean number of distinct clusters generated per recoil event was evaluated as shown in Figure 3-5. It is apparent that, within the resolution of the imposed recoil energy grid, the threshold for sub-cluster formation lies at approximately 10 keV in GaAs. Visual inspection of 10 keV recoil-induced defect maps confirmed the presence of characteristic features of sub-cluster breakup—namely the co-existence of two regions of high defect density that are separated by a distance on the order of, or larger than, the dimensions of each high-density region, with the possible inclusion of linear chains of defects linking the regions. The assessed 10 keV threshold exhibits good agreement with molecular dynamics (MD) based sub-cluster threshold estimates for metallic elements of a similar atomic number to Ga and As [9].

Next, the parameter $r_a$ in Eq. (2.1) was varied, and the behavior of the subtractive clustering algorithm-derived curves of cluster center number versus energy (see Figure 3-6) was scrutinized to identify the value of $r_a$ at which consistency is achieved with the RDF-based estimate of the sub-cluster formation threshold energy. At low recoil energies, the number of cluster centers ascertained via the subtractive clustering algorithm can be inaccurate, partly due to the increasingly ill-defined nature of a defect cluster as the recoil energy is reduced to a point where few defects are generated. In particular, below a recoil energy of a few hundred eV in GaAs, only a few defects are extant in the maps and the clustering algorithm may identify individual defects as comprising distinct clusters in and of themselves. Therefore, the portions of the curves in Figure 3-6 that are linearly increasing as a function of recoil energy (in log-log space) are perceived as the physically meaningful portions. This interpretation is in agreement with the functional behavior observed in residual defect clusters from MD simulations [9].

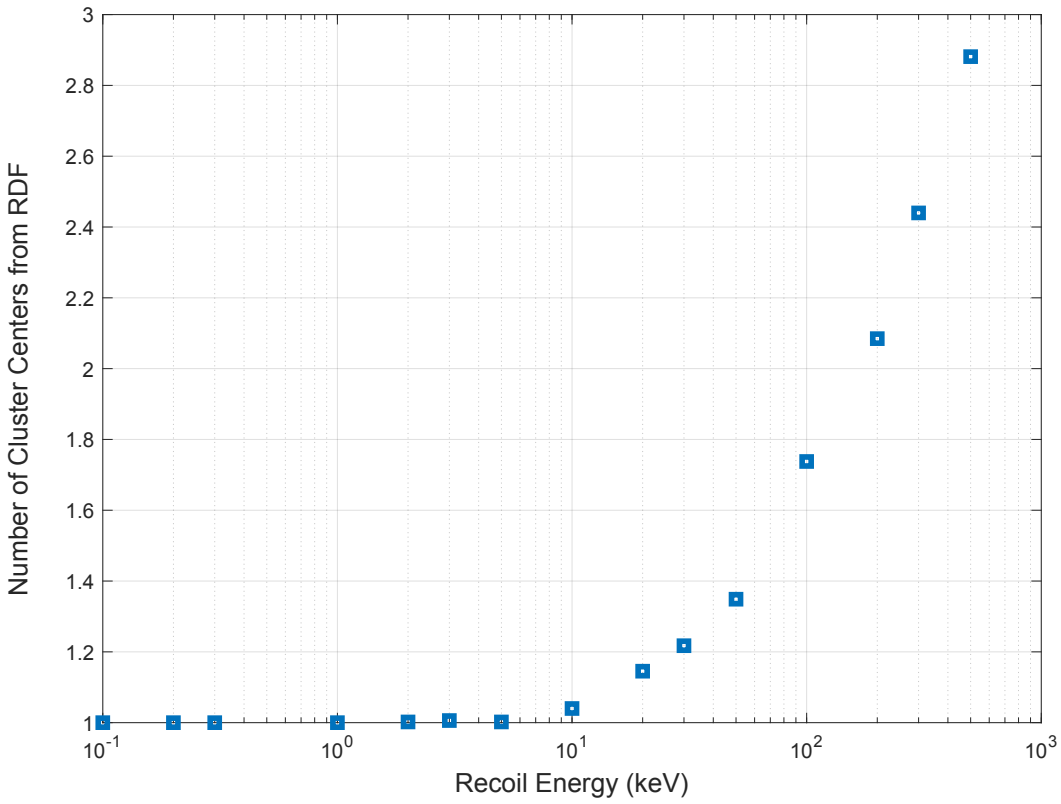


**Figure 3-5. Mean number of cluster centers versus recoil energy in GaAs, as identified using RDF analysis**

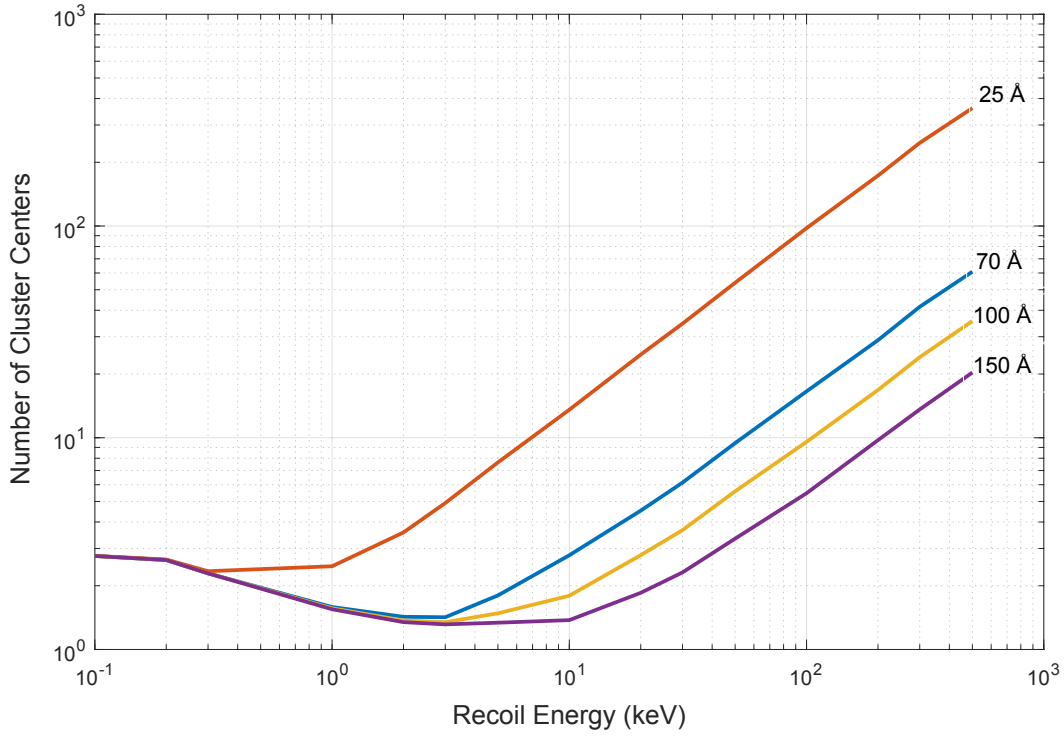


**Figure 3-6. Mean number of cluster centers versus recoil energy in GaAs, as evaluated using the subtractive clustering algorithm. Curves are labeled by value of $r_a$ (see Eq. (2.1)).**

By extrapolating the linear portions of the constituent curves of Figure 3-6 to unity on the ordinate axis, comparisons may be drawn to the threshold energy for sub-cluster formation as derived from Figure 3-5. For gallium arsenide, $r_a \approx 150$ Å produces a close match. Spatial analysis of defects clusters in gallium arsenide as generated using the Transport of Ions in Matter (TRIM) code [10] yields a mean sub-cluster size asymptotically approaching roughly 150 Å as recoil energy increases beyond 75 keV; substantially smaller clusters are reported below that energy. Thus, 150 Å is assessed as a reasonable choice for $r_a$ at recoils energies at which multiple, distinct defect clusters would occur with high probability.

With the parameter $r_a$ assigned a value and the degree-of-membership information integrated into the fitting process via the $exp(-2)$ cutoff for cluster affiliation, the ellipsoidal fitting process is ready to be deployed on arbitrary defect maps. Examples of fitted maps are given in Figure 3-7 – Figure 3-8 at a 50 keV recoil energy and in Figure 3-9 – Figure 3-11 at a 500 keV recoil energy. All distances are in angstroms.

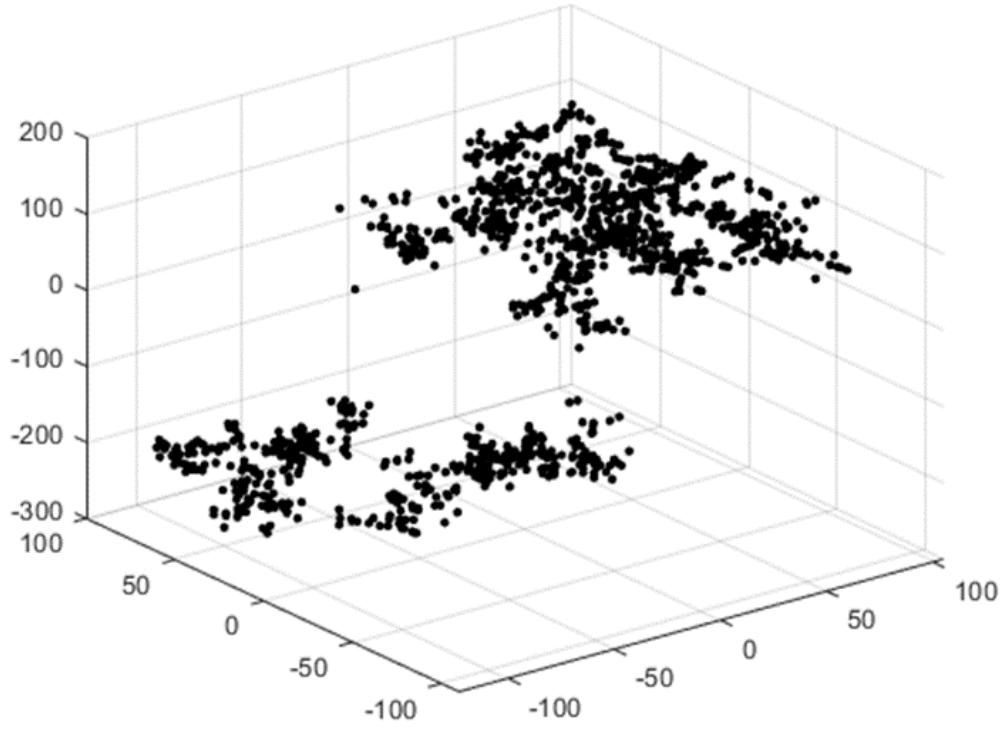


**Figure 3-7. Candidate defect map from 50 keV recoil**

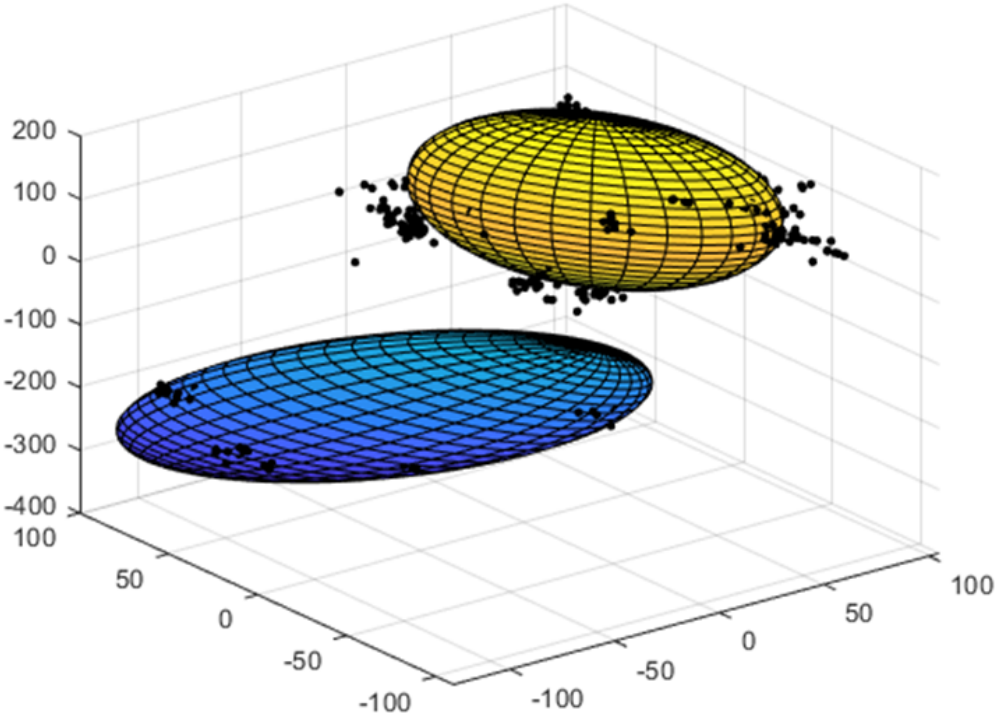


**Figure 3-8. Ellipsoidal sub-cluster fit to candidate defect map from 50 keV recoil**

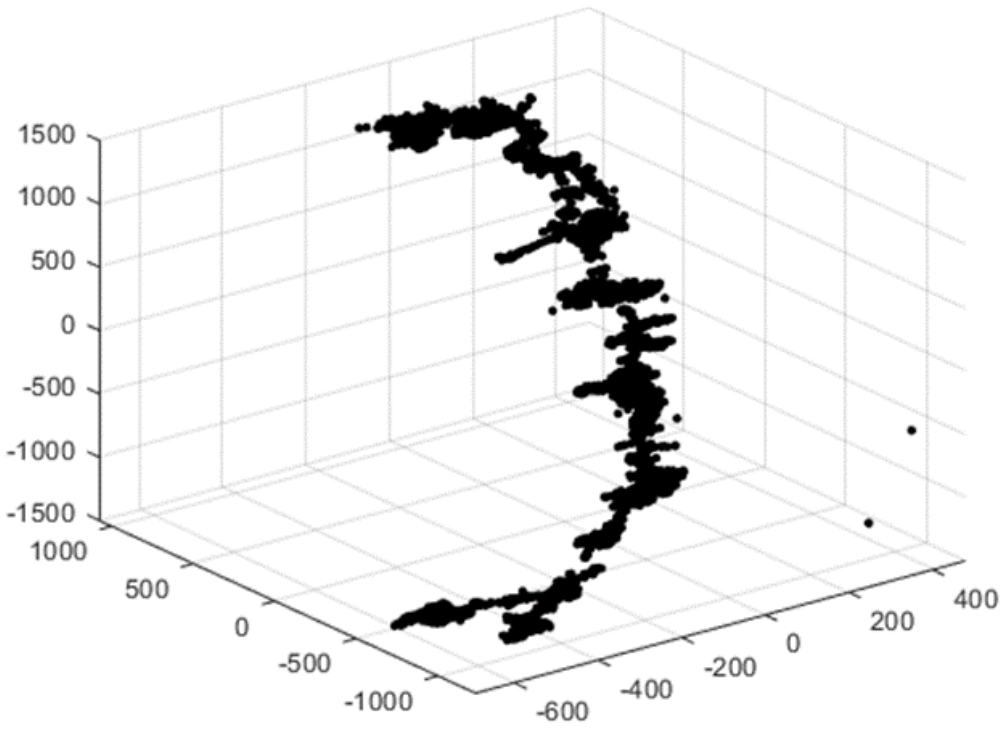


**Figure 3-9. Candidate defect map from 500 keV recoil**

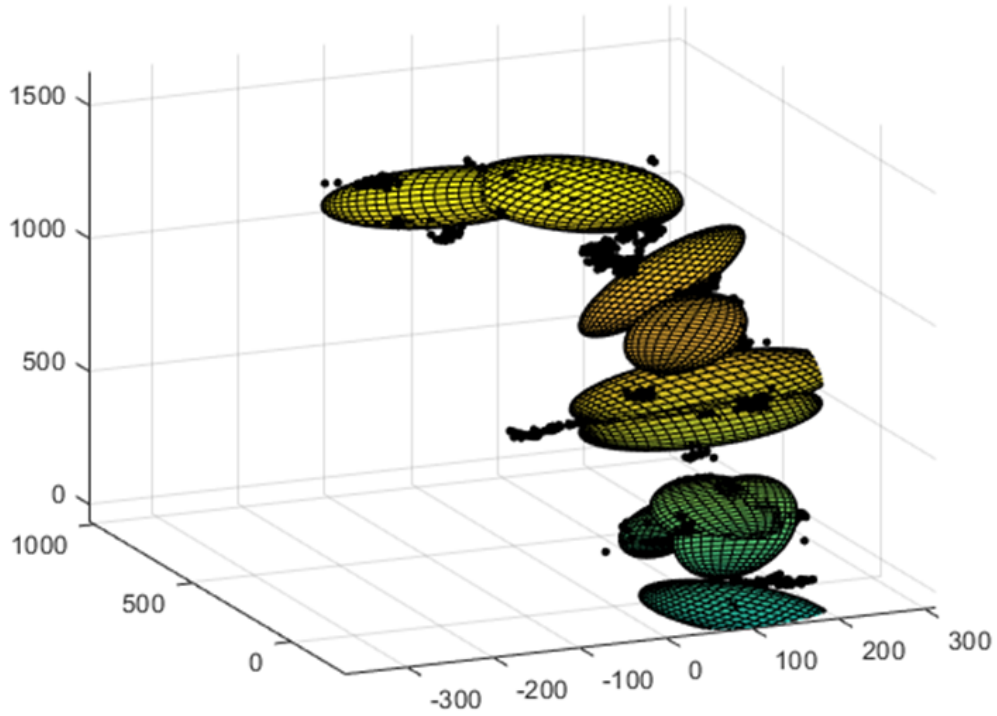


**Figure 3-10. Ellipsoidal sub-cluster fit to candidate defect map from 500 keV recoil: Upper portion**

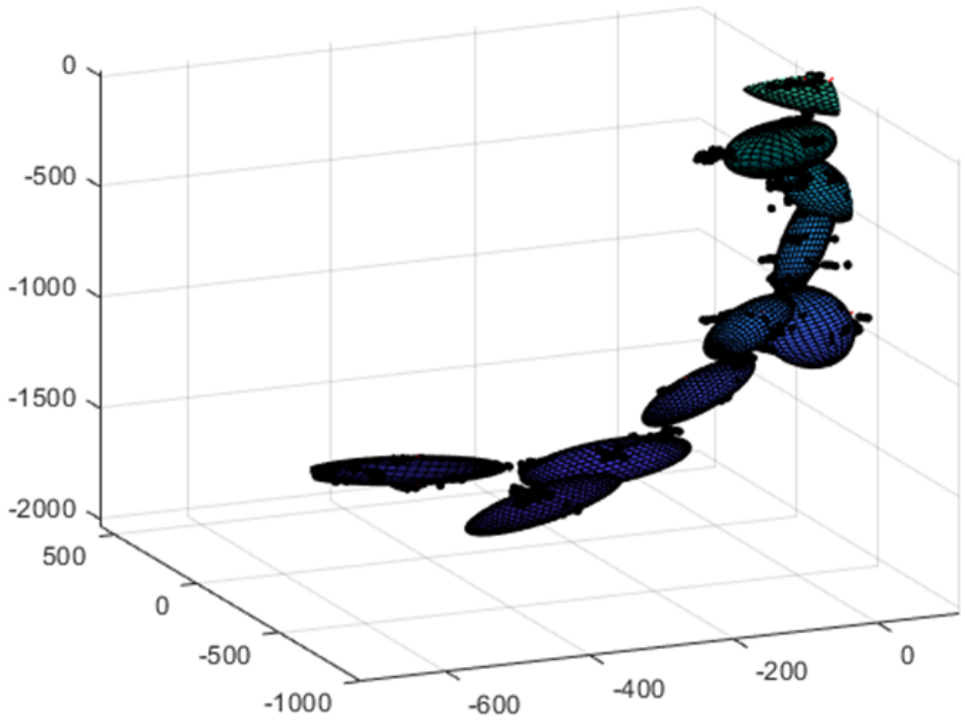


**Figure 3-11. Ellipsoidal sub-cluster fit to candidate defect map from 500 keV recoil: Lower portion**

This page left blank

# 4. DEFECT MAP VOLUME ESTIMATES IN GALLIUM ARSENIDE

With the ellipsoidal sub-cluster fitting model fully parameterized for gallium arsenide, the mean volume of a defect map was assessed as a function of recoil energy. Starting at a recoil energy of 10 keV (i.e. the approximate threshold energy of sub-cluster formation in GaAs), the fitting algorithm was applied to a wide variety of clustering realizations in accordance with the sampling scheme laid out in Table 3-1. For each realization, the defect map volume was defined as the aggregate volume of all $2\sigma$ ellipsoids identified under the PCA fitting scheme. This definition introduces the possibility that certain regions of the 3D space will be counted multiple times if the fitted ellipsoids overlap therein.

Comparisons were drawn against volume estimates obtained through two independent approaches, namely 1) fitting a single 2-sigma ellipsoid to the entire defect map, and 2) computing the convex hull [11] of the set of defect points. An example of a convex hull of a point defect map is given in Figure 4-1. The mean volumes evaluated using the three methodologies are illustrated in Figure 4-2 as a function of recoil energy. Good agreement is evident up to about 100 keV, above which the ellipsoidal sub-cluster fitting model branches off from the other two. Approximately an order-of-magnitude difference is observed at the highest recoil energy (500 keV). The origin of the difference lies in the inability of the relatively simple convex hull or single-ellipsoid fits to envelope the defects without also incorporating large swaths of "empty" (defect-devoid) space when many sub-clusters coexist in a complicated geometry. Thus, GaAs cluster volume calculations based on the aforementioned schemes will be prone to severe overestimation of the mean volume in the limit of high recoil energy. Considering that recoil energies of several hundred keV are achievable in GaAs in the presence of fission spectrum or 14-MeV neutrons, the differences amongst the models assume a practical significance.

The comparatively minor differences in volume between the convex hull and single-ellipsoid models are elucidated in Figure 4-3, which shows a histogram of the volume ratio of the two models over the energy range of 1000 eV to 500 keV (covering a total of 6000 sampled defect maps). Aside from a systematic offset of the convex hull fits towards slightly higher volumes, the occasional presence of "orphan defects" — i.e. defects separated from any sub-cluster by distances large in comparison to inter-cluster spacings, examples of which can be spotted in the lower-right corner of Figure 3-9— create a tail in the histogram distribution due to the algorithmic requirement that the convex hull volume incorporate every defect within a closed geometric form. Conversely, the "contour-hugging" nature of the convex hull mitigates the inclusion of defect-devoid, inter-cluster volumes in other cases. While single-ellipsoid fits are also influenced by orphan defects, the degree of influence is weighted by the (normally quite small) proportion of the latter versus the total defect population. Orphan defects are discounted entirely in the ellipsoidal sub-cluster fitting model as a consequence of the imposition of the degree-of-membership cutoff.

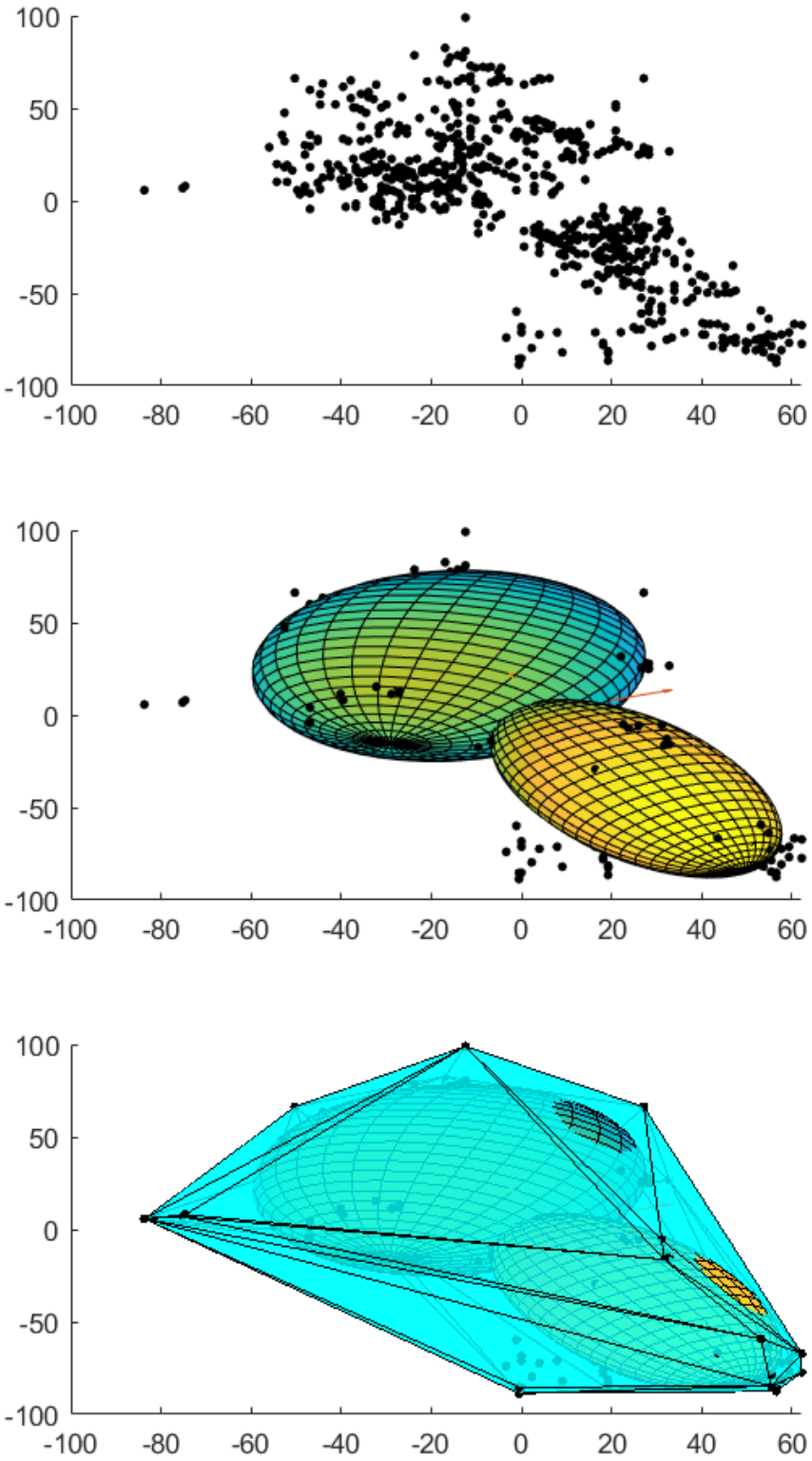


**Figure 4-1. Defect map from a 20 keV recoil in GaAs (top panel), fitted with sub-cluster 2-sigma ellipsoids (middle panel), and overlaid with the convex hull (bottom panel). Distances are in angstroms.**

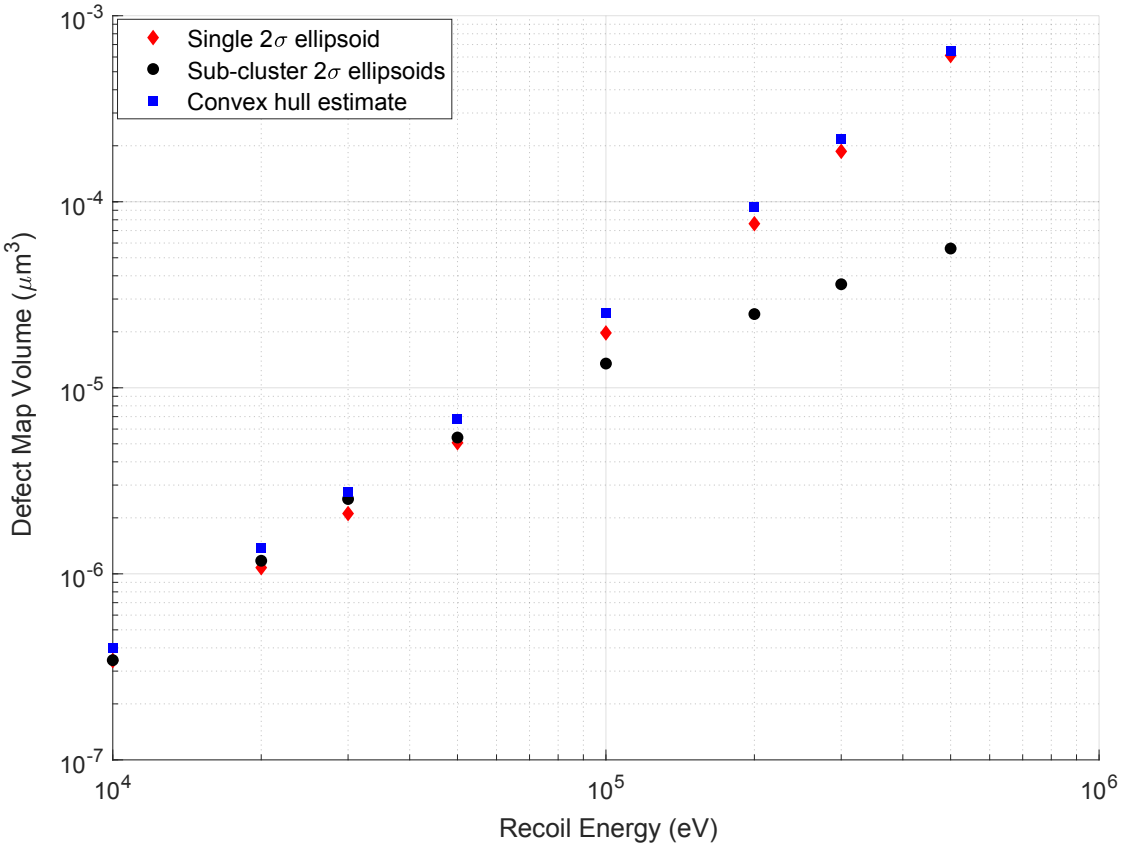


**Figure 4-2. Calculated mean volume of defect maps versus recoil energy in GaAs as a function of volume estimation methodology**

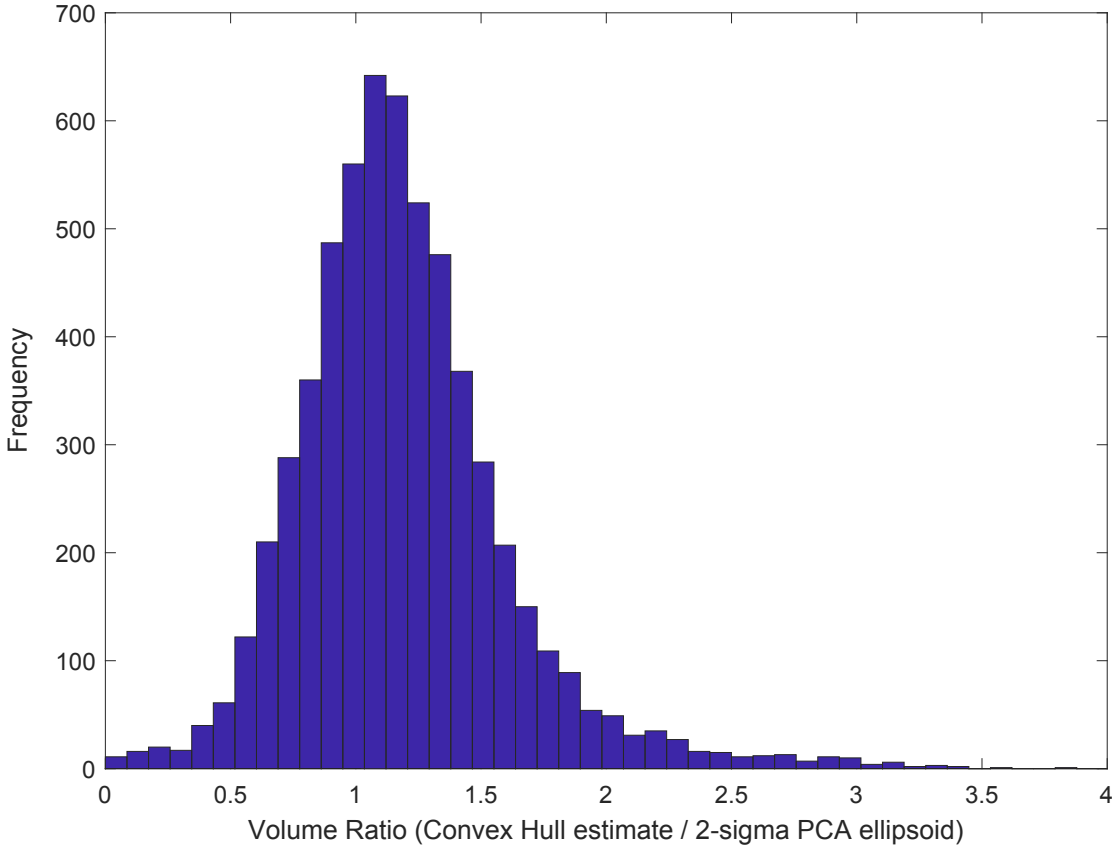


**Figure 4-3. Histogram of ratio of convex hull versus single 2-sigma ellipsoid estimate of cluster volume in the recoil energy range of 1000 eV to 500 keV.**

# 5. CONCLUSIONS

A methodology has been devised to fit the geometric contours of a defect map—consisting of one or more distinct clusters—by employing principal component analysis (PCA) to evaluate a set of surrogate ellipsoids. Specifically, the number of cluster centers was determined through a subtractive clustering algorithm, and the cluster center positions were optimized using c-means clustering analysis with a degree-of-membership value between 0 and 1 assigned to each defect vis-à-vis each cluster. This fuzzy membership value was then made binary by establishing a cutoff value of *exp(-2)* for inclusion in the PCA-fitted ellipsoid for each respective cluster. While the described fitting process is generalizable to any material, it was applied explicitly to GaAs in this study via the selection of an $r_a$ parameter value of 150 Å within the subtractive clustering algorithm to ensure consistency with the threshold energy for sub-cluster formation in GaAs. The sub-cluster threshold energy itself was set at 10 keV based on a separate analysis of radial distribution function behavior versus recoil energy.

The parameterized model for GaAs was utilized to compute the mean volume of quasi-stable defect maps obtained from the MARLOWE code as a function of recoil energy between 10 keV and 500 keV, where the latter energy lies at the upper end of the spectrum of recoil energies expected in GaAs from fission neutron bombardment. Comparisons were drawn against convex hull and single-ellipsoid fits to the point defect map, which represent simple, generic models that do not explicitly account for the existence of defect sub-clusters. The sub-cluster ellipsoidal fitting scheme was shown to begin to deviate from the two reference models at a recoil energy of around 100 keV, culminating in a difference of roughly an order of magnitude at 500 keV. Given the accommodations made within the sub-cluster fitting model to spatial defect distributions characteristic of PKA-induced displacement damage, the reference models are concluded to overestimate the defect map volume due to the incorporation of sizable swaths of intervening, defect-free space.

While the actual extent of any inter-cluster interaction effects will be dependent on the detailed geometries of the clusters as well as the background concentrations of defect-trapping impurities, the methodology put forward in this study is posited to be an appropriate starting point for estimating the neutron fluence at which such effects might become significant. Aside from this particular application, the defined methodology provides a framework for users to extract other reduced metrics from complex defect map geometries that are characteristic of materials of interest.

# REFERENCES


[1] R. Yager and D. Filev. *Journal of Intelligent & Fuzzy Systems*, **2**, No. 3, pp. 209-219 (1994).

[2] J. C. Bezdek, R. Ehrlich, and W. Full. *Computers and Geosciences*, **10**, No. 2-3, pp. 191-203 (1984).

[3] M. Hou. *Phys. Rev. B*, **31**, 4178 (1985).

[4] M. T. Robinson. *Phys. Rev. B*, **40**, 10717 (1989).

[5] M. T. Robinson. *Nucl. Instr. Meth. Phys. Res. B*, **48**, 408 (1990).

[6] M. T. Robinson. *Nucl. Instr. Meth. Phys. Res. B*, **67**, 396 (1992).

[7] M. T. Robinson. *Nucl. Instr. Meth. Phys. Res. B*, **115**, 549 (1996).

[8] B. D. Hehr. "Verification and Validation of Defect Production Metrics in NuGET", Sandia Technical Report SAND2016-9817, (2016).

[9] A. De Backer *et al. EPL*, **115**, 26001 (2016).

[10] E. V. Kiseleva and S. V. Obolenskii, *Russian Microelectronics*, **35**, No. 5, 322 (2006).

[11] F. P. Preparata and M. I. Shamos. *Computational Geometry.* Springer, New York, NY, pp. 95 – 149, (1985).

# DISTRIBUTION

**Email—Internal**

| Name | Org. | Sandia Email Address |
|---|---|---|
| Patrick J. Griffin | 01000 | pjgriff@sandia.gov |
| Gyorgy Vizkelethy | 01866 | gvizkel@sandia.gov |
| William R. Wampler | 01866 | wrwampl@sandia.gov |
| | | |
| Technical Library | 01177 | libref@sandia.gov |

This page left blank

This page left blank

Sandia National Laboratories

Sandia National Laboratories is a multimission laboratory managed and operated by National Technology & Engineering Solutions of Sandia LLC, a wholly owned subsidiary of Honeywell International Inc. for the U.S. Department of Energy's National Nuclear Security Administration under contract DE-NA0003525.